

# Forced ignition of premixed cool and hot DME/air flames in a laminar counterflow

Yan Wang<sup>1</sup>, Shumeng Xie<sup>1</sup>, Hannes Böttler<sup>2</sup>, Xinyi Chen<sup>2</sup>, Arne Scholtissek<sup>2</sup>, Christian Hasse<sup>2</sup>, Zheng Chen<sup>1,\*</sup>

<sup>1</sup>SKLTCS, HEDPS, CAPT, College of Engineering, Peking University, Beijing, China

<sup>2</sup>Department of Mechanical Engineering, Simulation of reactive Thermo-Fluid Systems, Technical University of Darmstadt, Otto-Berndt-Str. 2, 64287 Darmstadt, Germany

## 1 Introduction

For large hydrocarbon fuels, the low temperature chemistry (LTC) [1] can induce two-stage autoignition and cool flame, which might occur in homogeneous charge compression ignition (HCCI) engines and spark-assisted compression ignition (SACI) engines [2]. Previous studies showed that the LTC-induced cool flame can substantially accelerate the subsequent hot flame propagation [3, 4] and reduce the minimum ignition energy at certain conditions [5]. Since the premixed cool flame speed is much slower than that of the hot flame, the cool flame is usually caught up and merged by the hot flame [3, 4]. Consequently, it is difficult to establish a steady premixed cool flame [6]. Moreover, the forced ignition of premixed cool flame is not well understood. This motivates the present study, which aims to understand the ignition and stabilization of premixed cool flame in a counterflow configuration.

Dimethyl ether (DME) is one of the promising alternative fuels and its LTC has been extensively studied. Moreover, the cool flame in DME/air mixtures was investigated in many previous studies. For examples, Zhang et al. [3] simulated the ignition and propagation of premixed cool flame in a static DME/air mixture. Yang et al. [5] found that the minimum ignition energy for cool flame is much lower than that for hot flame in DME/air mixtures. Zhao et al. [7] successfully established a quasi-steady premixed cool flame in both numerical simulations and experiments, by reducing the intermediate residence time in the counterflow configuration.

All the above studies were limited to one-dimensional configuration and did not consider the influence of multi-dimensional flow on the ignition and propagation/stabilization of premixed cool flame. In this study, we shall consider the forced ignition of premixed cool and hot DME/air flames in a laminar counterflow. Specifically, the flame kernel evolution and the critical conditions for cool and hot flame ignition shall be investigated.

## 2 Model and numerical specifications

The transient forced ignition process of DME/air mixture in a 2D axisymmetric counterflow is schematically shown in Fig. 1. An expanding flame is induced by forced ignition at the stagnation point. It propagates outwardly and becomes an ellipsoid due to the counterflow. Finally, the twin premixed

flames are stabilized in the counterflow. The transient ignition process is simulated using the in-house solver EBI-DNS developed by Zirwes et al. [8, 9] based on OpenFOAM [10]. The detailed kinetic model developed by Zhao et al. [11] is used. This kinetic model was extensively validated and widely used in previous studies [3, 4, 12]. The computation domain is  $20 \times 10 \text{ mm}^2$  which is covered by uniform wedge grid of  $\Delta r = \Delta z = 25 \text{ }\mu\text{m}$ . A stoichiometric DME/air mixture of 450 K with uniform velocity  $U_{in}$  is fixed on the top inlet boundary. The ambient pressure is set to 5 atm to accelerate LTC reactions. The global strain rate  $a_g$  of the counterflow is:

$$a_g = \frac{2U_{in}}{L} \left( 1 + \frac{U_t \sqrt{\rho_t}}{U_b \sqrt{\rho_b}} \right) = \frac{4U_{in}}{L},$$

Before ignition, the mixture is chemically frozen and the flow field reaches a steady state. The ignition kernel center is set at the stagnation point ( $r=z=0$ ). The mixture is ignited by energy deposition given by the following source term in the energy equation:

$$\dot{q}_{ign} = \frac{3E_{ign}}{4\pi R_{ign}^3 \tau_{ign}} \exp\left(-\frac{\pi}{4} \left(\frac{R}{R_{ign}}\right)^6\right), \text{ for } 0 < t < \tau_{ign},$$

where  $E_{ign}$  is the total ignition energy,  $R_{ign}$  is the radius of energy deposition, and  $\tau_{ign}$  is the deposition duration. We use  $R_{ign} = 500 \text{ }\mu\text{m}$  and  $\tau_{ign} = 200 \text{ }\mu\text{s}$  unless otherwise specified.

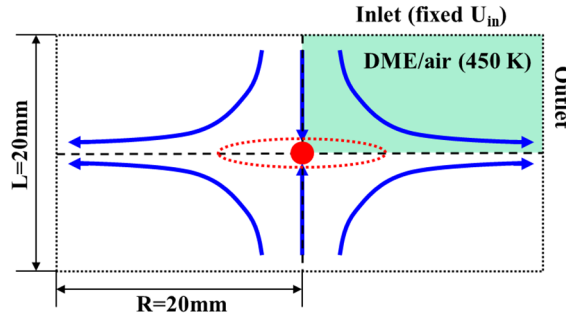


Figure 1 Schematics of the forced ignition in the counterflow.

### 3 Results and discussion

#### 3.1 The evolution of cool flame kernel in the counterflow

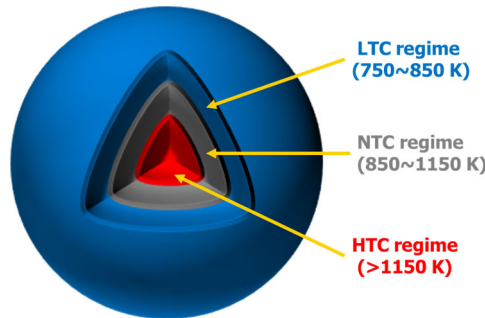


Figure 2 Schematics of low and high temperature chemistry thermal runaway and the corresponding temperature ranges.

Cool flame only appears when the ignition energy and strain rate are in a certain range. A small ignition energy cannot successfully ignite the mixture, whereas a large ignition energy directly ignites a hot flame rather than a cool flame. The ignition process consists of two parts: thermal runaway and flame kernel propagation. Figure 2 shows the different regimes of ignition kernel and corresponding temperature ranges. Low temperature chemistry shows highest activity when the temperature is in the range of 750~850 K. Due to the negative temperature coefficient of DME, the temperature range of

850~1150 K corresponds to low reactivity. For temperature above 1150 K, the high temperature chemistry (HTC) becomes dominant. Therefore, the thermal runaway of cool and hot flame occurs in different ranges of temperature and strongly depends on the ignition energy. It is noted that the hot flame is much faster than the cool flame. Therefore, once HTC thermal runaway is induced, the hot flame rapidly propagates and it catches up and merges with the leading cool flame. Only with a proper ignition energy, the LTC thermal runaway can be induced successfully.

Figure 3 shows a typical case for cool flame ignition and propagation at  $E_{ign}=0.825$  mJ and  $a_g=40$  s<sup>-1</sup>. After the LTC thermal runaway, the stretch rate begins to influence the cool flame kernel propagation. As figure 3 shows, the propagation of cool flame fronts and corresponding density displacement speed at different positions. There are three stages for the cool flame kernel propagation. The first stage is the ignition energy assisted propagation ( $t=0\sim 4$  ms). The cool flame propagates outwardly, whereas the density weighted displacement decreases. The second stage is deformation process ( $t=4\sim 26$  ms), in which the effect of ignition gradually decays and the counterflow changes the flame shape from sphere to ellipsoid. The counterflow pushes the flame backwards, flattens the flame shape and enhances the flame speed in axial direction. While the high curvature intensifies the radical loss and restrains the cool flame propagation in radial direction. The third stage is the transition to a twin counterflow flame ( $t>26$  ms). The curvature in both axial and radial directions decreases as flame expands outwardly, and the displacement speed increases.

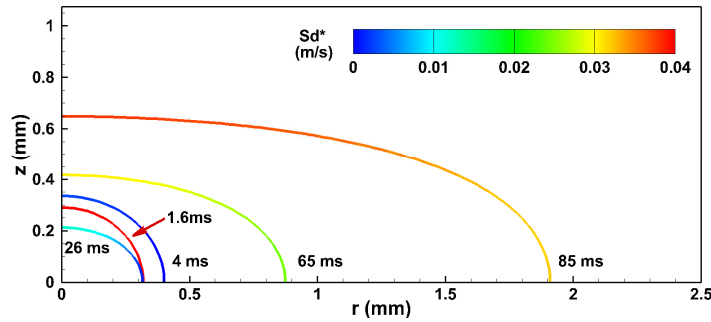


Figure 3 The cool flame propagation for  $E_{ign}=0.825$  mJ and  $a_g=40$  s<sup>-1</sup>.

Here we focus on the evolution of flame on axial (i.e.,  $r=0$ ) and radial (i.e.,  $z=0$ ) direction. Figure 4 shows the change of density weighted displacement speed  $S_d^*$  with local stretch rate  $K$ . Compared with the spherical flame kernel evolution, counterflow enhances the flame displacement in axial direction but suppresses the flame displacement in radial direction. The flame propagation in axial direction shows three regimes: the ignition energy assisted propagation ( $A_z B_z$ ), the unsteady transition propagation ( $B_z C_z$ ), the normal flame propagation ( $C_z D_z$ ). This evolution process is similar to that of a spherical flame but shows a higher turning point  $B_z$ . However, the flame propagation in radial direction only shows the first two regimes which indicates a slower evolution and a sustaining unsteady propagation.

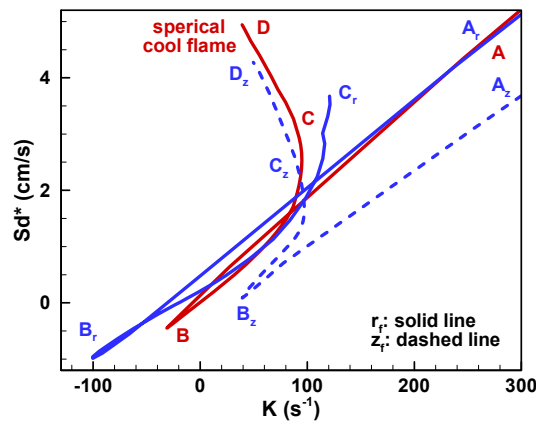


Figure 4 Change of density weighted displacement speed  $S_d^*$  with local stretch rate  $K$ .

### 3.2 Influence of strain rate on flame transition

Figure 5(a) shows the change of maximum temperature with the same ignition energy but different strain rates. The flame kernel finally extinguishes with a large strain rate of  $a_g=200 \text{ s}^{-1}$ . We find that the global strain rate not only influences the cool flame kernel propagation, but also determines the occurrence of second stage ignition. After the cool flame kernel propagates outwardly, a second stage ignition is spontaneously induced with a strain rate of  $a_g=20 \text{ s}^{-1}$ , resulting the double flame structure with a hot flame following the leading cool flame. The double flame structure is not observed for relatively high strain rate of  $a_g=100 \text{ s}^{-1}$ .

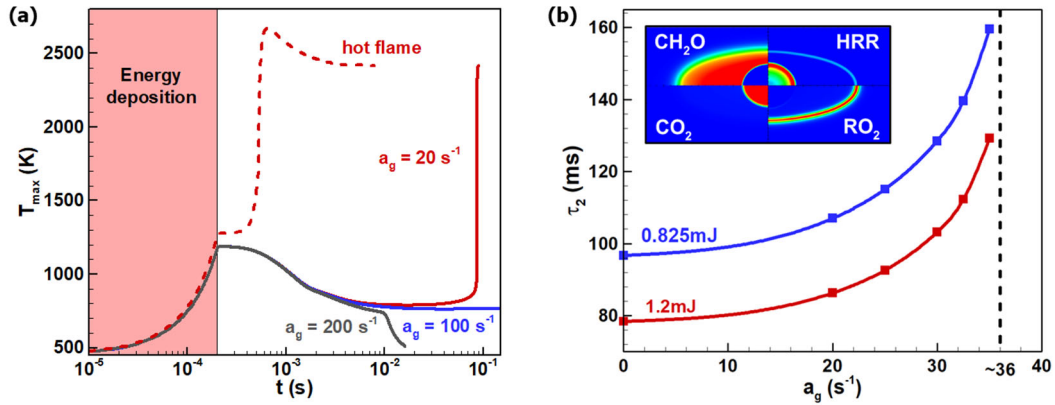


Figure 5 (a) The evolution of the maximum temperature for different strain rates of  $a_g=20, 100$  and  $200 \text{ s}^{-1}$  with the same ignition energy of  $E_{\text{ign}}=1.15 \text{ mJ}$  (solid lines). The evolution of hot flame with  $a_g=100 \text{ s}^{-1}$  and  $E_{\text{ign}}=1.25 \text{ mJ}$  is also plotted for reference (dashed line). (b) Change of the second-stage ignition delay time with global strain rate and the double flame structure in counterflow.

Figure 5(b) shows that the second stage ignition under small strain rate is similar to that in spherical flame ignition. The hot flame is induced at the stagnation point, then it propagates outwardly and finally merges with the cool flame. There are two heat release rate peaks: cool flame ( $10^8 \text{ Jm}^{-3}\text{s}^{-1}$ ) and hot flame ( $10^{11} \text{ Jm}^{-3}\text{s}^{-1}$ ). The cool flame front can also be represented by the peak of mass fraction of  $\text{RO}_2$  ( $\text{CH}_3\text{OCH}_2\text{O}_2$ ). Behind the cool and hot flame fronts,  $\text{CH}_2\text{O}$  and  $\text{CO}_2$  are produced respectively. Interestingly, there exists a critical strain rate ( $a_g \sim 36 \text{ s}^{-1}$ ) where the second stage ignition delay time increases to infinity. Above this limit, no hot flame is induced and a steady cool flame is formed eventually. Two ignition energies of  $E_{\text{ign}}=0.825 \text{ mJ}$  (close to the MIE for cool flame) and  $1.2 \text{ mJ}$  (close to the MIE for hot flame) are considered. We find that a large ignition energy reduces the second-stage ignition delay time but does not change the critical strain rate as shown in Fig. 5(b).

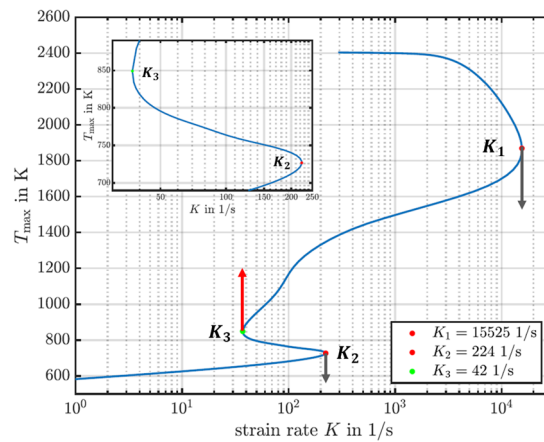


Figure 6 S-curve of premixed DME/air counterflow flames at 450 K and 5 atm.

The second stage ignition and the critical strain rate can be explained by 1D calculation of ignition and extinction in a counterflow. Figure 6 shows the three critical strain rates respectively corresponding to the hot flame extinction (HFE) limit at  $K_1$ , the high-temperature ignition (HTI) limit at  $K_2$  and the cool flame extinction (CFE) limit at  $K_3$ . The line between  $K_2$  and  $K_3$  represents the regime where a steady cool flame can exist. The transition point  $K_2$  shows a minimum strain rate limit, below which the cool flame finally transits into a hot flame. This limit is close to 2D simulation.

### 3.3 The ignition regime

Finally, we investigate the minimum ignition energy for different strain rate. Figure 7 shows the MIE for both cool and hot flames. For the cool flame, the MIE increases monotonically with the strain rate and increases sharply around the critical strain rate around  $a_g=110 \text{ s}^{-1}$ , above which only hot flame can be ignited. Depending on the ignition energy and strain rate, there are four regimes as shown in Fig. 7, which respectively corresponds to the four evolutions in Fig. 5(a). In regime I, only hot flame can appear. In regime II, the cool flame can be ignited and a hot flame subsequently appears. Subsequently, the hot flame catches up and merges with the leading cool flame. In regime III, the cool flame is ignited and stabilized in the counterflow and there is no hot flame. In regime IV, the ignition energy is too low to ignite any flame.

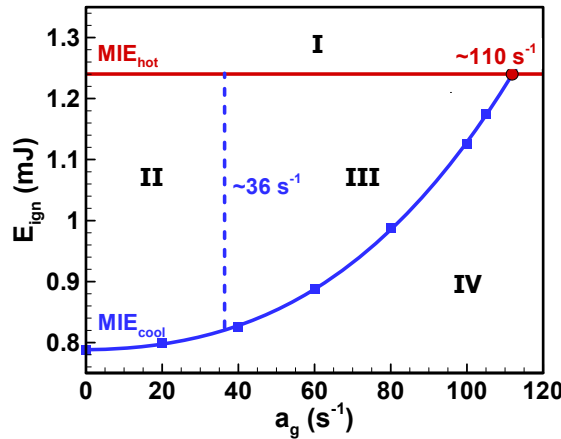


Figure 7 Ignition regime diagram of DME/air mixture at 450 K and 5 atm in a counterflow.

Figure 8 summarizes the flame evolution for different ignition regimes.  $E_{hot}$  and  $E_{cool}$  respectively represent the MIE for LTC and HTC thermal runaway. With the ignition energy is higher than  $E_{hot}$ , the hot flame is directly induced and propagates outwardly. When the ignition energy is lower than  $E_{cool}$ , the thermal runaway fails. When the ignition energy is between  $E_{cool}$  and  $E_{hot}$ , a cool flame can be ignited successfully. Then the strain rate influences the flame propagation. A large strain rate intensifies the radical loss and restrains the flame propagation, leading to extinction. However, a small strain rate leads to a transition from cool flame to hot flame. Only with a moderate strain rate, a steady cool flame can be established.

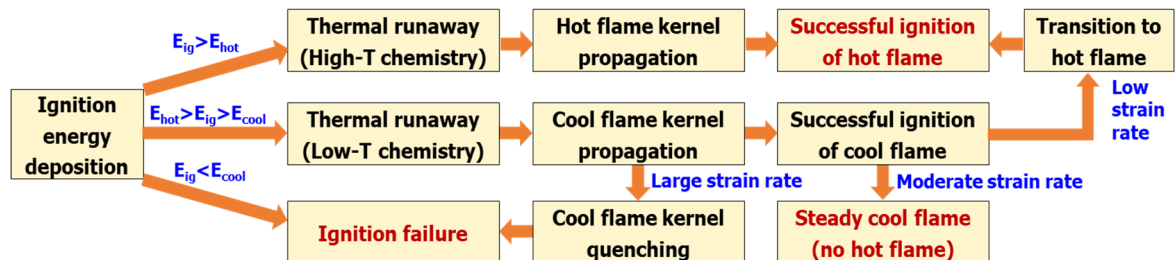


Figure 8 Ignition process with different ignition energies and strain rates.

## 4 Conclusions

In this study, 2D axisymmetric simulations considering detailed chemistry and transport are conducted to investigate the ignition of premixed cool and hot DME/air flames in a counterflow. The LTC and HTC thermal runaway, flame kernel propagation and transition from cool flame to hot flame are discussed. We find that the thermal runaway of LTC and HTC occurs at different regimes and times. After thermal runaway, the strain rate influences the flame kernel propagation and determines the transition from cool flame to hot flame. For cool flame, a large or small strain rate respectively leads to ignition failure and transition to hot flame. Only with a proper strain rate, a steady cool flame can be established. A regime diagram in terms of ignition energy and strain rate is proposed, and four regimes are identified and interpreted.

## Acknowledgements

This work was funded by NSFC, China (Nos. 521760965, 51861135309) and DFG, German (No. 411275182). We thank Drs. Thorsten Zirwes, Feichi Zhang, and Henning Bockhorn at Karlsruhe Institute of Technology for providing us their EBI-DNS code and Mr. Felix Rong at Technical University of Darmstadt for providing Fig. 6.

## References

- [1] F. Battin-Leclerc, Detailed chemical kinetic models for the low-temperature combustion of hydrocarbons with application to gasoline and diesel fuel surrogates, *Prog Energy Combust Sci* 34 (2008) 440-498.
- [2] Y. Ju, Understanding cool flames and warm flames, *Proc Combust Inst* 38 (2021) 83-119.
- [3] W. Zhang, M. Faqih, X. Gou, Z. Chen, Numerical study on the transient evolution of a premixed cool flame, *Combust Flame* 187 (2018) 129-136.
- [4] Y. Wang, H. Zhang, T. Zirwes, F. Zhang, H. Bockhorn, Z. Chen, Ignition of dimethyl ether/air mixtures by hot particles: Impact of low temperature chemical reactions, *Proc Combust Inst* 38 (2021) 2459-2466.
- [5] Q. Yang, P. Zhao, Minimum ignition energy and propagation dynamics of laminar premixed cool flames, *Proc Combust Inst* 38 (2021) 2315-2322.
- [6] C.B. Reuter, S.H. Won, Y. Ju, Experimental study of the dynamics and structure of self-sustaining premixed cool flames using a counterflow burner, *Combust Flame* 166 (2016) 125-132.
- [7] P. Zhao, W. Liang, S. Deng, C.K. Law, Initiation and propagation of laminar premixed cool flames, *Fuel* 166 (2016) 477-487.
- [8] T. Zirwes, F. Zhang, P. Habisreuther, M. Hansinger, H. Bockhorn, M. Pfitzner, D. Trimis, Quasi-DNS Dataset of a Piloted Flame with Inhomogeneous Inlet Conditions, *Flow, Turbu Combust* 104 (2020) 997-1027.
- [9] T. Zirwes, F. Zhang, J.A. Denev, P. Habisreuther, H. Bockhorn, Automated Code Generation for Maximizing Performance of Detailed Chemistry Calculations in OpenFOAM, in: W.E. Nagel, D.H. Kröner, M.M. Resch (Eds.) *High Performance Computing in Science and Engineering '17*, Springer International Publishing, Cham, 2018, pp. 189-204.
- [10] H.G. Weller, G. Tabor, H. Jasak, C. Fureby, A Tensorial Approach to Computational Continuum Mechanics Using Object Orientated Techniques, *Computers Phys* 12 (1998) 620-631.
- [11] Z. Zhao, M. Chaos, A. Kazakov, F.L. Dryer, Thermal decomposition reaction and a comprehensive kinetic model of dimethyl ether, *Int J Chem Kinet* 40 (2008) 1-18.
- [12] Y. Wang, W. Han, T. Zirwes, F. Zhang, H. Bockhorn, Z. Chen, Effects of low-temperature chemical reactions on ignition kernel development and flame propagation in a DME-air mixing layer, *Proc Combust Inst* 39 (2023) Available on line. <https://doi.org/10.1016/j.proci.2022.07.024>